Plasma screening effects on the electronic structure of multiply charged Al ions using Debye and ion-sphere models

Madhulita Das,[1,*] B. K. Sahoo,[2,†] and Sourav Pal[3]
[1]*National Institute of Technology, Rourkela, Odisha 469008, India*
[2]*Theoretical Physics Division, Physical Research Laboratory, Navrangpura, Ahmedabad 380009, India*
[3]*Indian Institute of Technology Bombay, Powai, Mumbai 400076, India*
(Received 6 April 2016; published 23 May 2016)

We analyze atomic structures of plasma-embedded aluminum (Al) atom and its ions in the weak- and strong-coupling regimes. The plasma screening effects in these atomic systems are accounted for using the Debye and ion-sphere (IS) potentials for the weakly and strongly coupled plasmas, respectively. Within the Debye model, special attention is given to investigate the spherical and nonspherical plasma screening effects considering in the electron-electron interaction potential. The relativistic coupled-cluster (RCC) method has been employed to describe the relativistic and electronic correlation effects in the above atomic systems. The variations in the ionization potentials (IPs) and excitation energies (EEs) of the plasma-embedded Al ions are presented. It is found that the atomic systems exhibit more stability when the exact screening effects are taken into account. It is also shown that in the presence of a strongly coupled plasma environment, the highly ionized Al ions show blueshifts and redshifts in the spectral lines of the transitions between the states with the same and different principal quantum numbers, respectively. Comparison among the results obtained from the Debye and IS models are also carried out considering similar plasma conditions.

DOI: 10.1103/PhysRevA.93.052513

I. INTRODUCTION

Electronic structures of atomic systems immersed in a hot and dense plasma environment may be remarkably different from their corresponding isolated candidates. Accurate estimation of the electronic structures of atoms or ions is one of the active fields of research in recent years for their wide range of applications [1–3]. The plasma may contain different charged species as well as free electrons. These charged particles can screen the atomic potential of the embedded atomic systems, resulting in deviations in the structures of the systems from their corresponding isolated systems. Owing to the complex nature of the potentials describing the electron-nucleus and electron-electron interactions, it is extremely difficult to carry out *ab initio* calculations of the electronic structures of the plasma-embedded atomic systems. Thus, to describe their structures conveniently, model atomic potentials are used which account for the plasma screening effects. The plasma environment can be classified into weakly and strongly coupled plasma, depending on the strength of its coupling constant Γ, which is the ratio of the Coulomb potential energy to the thermal energy. For weakly coupled plasma ($\Gamma \ll 1$; i.e., low density and high temperature), the screening effect can be appropriately described using the Debye model [1]. However, in the strongly coupled plasma ($\Gamma \gg 1$ implying high density and low temperature) the ion-sphere (IS) potential model [4] is the best suited model for accounting for plasma screening effects. Both the Debye and ion-sphere models have been successfully employed several times previously to describe the electronic properties of different plasma-embedded atomic systems [5–12]. The effect of nuclear charge screening by plasma free electrons is reciprocated in the form of ionization potential depression (IPD) or continuum lowering [13–16]. Other crucial spectral properties of atomic systems that are of immense interest are excitation energies (EEs), spectral line shifts, line broadenings, energy level crossings, etc. Accurate knowledge of these quantities is essential in describing the equation of state of plasma [17], finding out the opacity of an element in the astrophysical plasma [18,19], in understanding dynamics of atomic systems in the laser cooling and trapping of ions [20], inertial confinement fusion studies [21], etc.

These days many laboratory experiments are being performed in this regard. Recently, aluminum (Al I) and its different multicharged ions have been considered for the laboratory plasma experiments. In the Linac Coherent Light Source (LCLS) and free-electron-laser (FEL) experiments, Al is used as a common target material. Riordan and Pearlman [22] had characterized the absorption spectroscopy of a cold and dense Al plasma using a pulsed soft x-ray continuum backlighting source. In their experiment, they characterized the L-shell spectra of Al IV and Al V at a plasma temperature and electron density of 12 eV and 0.6×10^{21} cm^{-3}, respectively. Similarly, Pérez-Tijerina *et al.* [23] had used a wide field spectrograph to analyze the behavior of the laser-produced Al plasma by measuring the linewidths of the singly (Al II) and doubly (Al III) ionized Al. Ciobanu *et al.* [24] had also studied the spectroscopy of Al plasma by using the second (532 nm) harmonic of a Q-switched pulsed Nd-YAG laser and had observed many line intensities. In other works, Hoarty *et al.* [25] and Ciricosta *et al.* [26] experimentally studied the influence of a hot and dense plasma environment on the spectroscopy of Al atoms and had reported its IPDs. Ciricosta *et al.* had used x-ray free-electron lasers to analyze the K-edge spectra of solid-density Al plasma with temperature up to 180 eV. In a different experiment, the newly commissioned Orion laser system was used to investigate the Al samples with a varying plasma density of 1–10 g/cc and electron temperature of 500 eV and 700 eV to study the IPD as a

*physics.madhulia@gmail.com
†bijaya@prl.res.in

function of plasma density [25]. Also, a number of theoretical studies on Al plasma have been carried out because of its experimental interest. Zeng *et al.* [27] had performed extensive calculations of the x-ray transmission spectra for the high-power laser-produced Al plasma in local thermodynamic equilibrium (LTE) by employing a configuration interaction (CI) scheme and the R-matrix method with the detailed-term-accounting approximation. Feng *et al.* [28] had theoretically simulated the x-ray emission spectra of Li-like Al ion by using the collisional radiative model. Preston *et al.* [29] had simulated the emission spectra of the hot and dense Al plasma using the Stewart-Pyatt (SP) and modified Ecker-Kröll (mEK) models. Very recently, Kiyokawa [30] calculated the radiative opacity of the Al plasma in LTE by using the time-dependent density-functional theory (TDDFT) at temperature $T = 20$ eV and density 0.01 g/cm^3. The strongly coupled plasma is mostly seen in the highly evolved stars, interior of the Jovian planets, explosive shock tubes, laser-produced plasma, and inertial confinement fusion plasmas [4,31–33]. Most of these studies have been carried out in the Debye model formalism. However, there has been no theoretical investigation of the strongly coupled Al plasma carried out in the IS model framework. Nevertheless, it appears from a large number of studies that probing structures of Al plasma are of ample interest to both experimentalists and theoreticians working in this field.

The primary interest of the present work is to carry out an *ab initio* investigation of electronic structures of Al and some of its ions in both a weakly and strongly coupled plasma environment. In most of the previous studies, the electronic structures of Al plasma have been investigated using many-body methods which account for the electron correlation effects inefficiently. Accurate calculations in the atomic systems with more than four electrons require a many-body method that is capable of including electron correlation effects rigorously. Again, the relativistic effects in these ions are usually large. In this work, we employ a relativistic coupled-cluster (RCC) method to carry out the theoretical investigations in the considered atomic systems. The RCC method is an all order perturbative method that obeys the size extensivity and size consistent behavior [34,35]. In weakly coupled plasma, we consider the Debye-screened potential instead of the usual atomic potential in the RCC method to describe the change in the spectroscopic properties of the plasma-embedded Al ions. The approach in which the screening effect is taken into account only through the nuclear potential is referred to as the spherical Debye (SD) potential approximation. However, plasma free electrons may also play an important role in the screening of bound electron-electron interaction term in the potential. The approach in which both nuclear and electronic charge screenings are considered explicitly is denoted as nonspherical Debye (NSD) potential approximation. Owing to the complexity in the consideration of the NSD potential approximation in a perturbative approach, this is rarely applied in the investigation of the electronic structure of plasma-embedded atomic systems. The SD potential approximation may provide reasonably accurate results in the H-like, He-like, and Li-like atomic systems, where there are not many electrons present. However, it has been found that consideration of NSD potential approximation can lead to very interesting results in the evaluations of the orbital energies and transition probabilities in plasma-embedded atomic systems [36,37]. Recently, Gutierrez and Diaz-Valdes [38] also showed that NSD potential gives rise to large collision strengths compared to the SD potential approximation. In this work, we intend to make a comparative analysis of results considering both the SD and NSD potentials through our RCC method. Similarly, the effect of the strongly coupled plasma environment on the atomic structure of Al ions is being investigated by considering the IS potential in the RCC method. Again, we consider a few cases with the given experimental conditions of plasma and investigate IPDs and EEs of the Al III and Al XI ions in both the NSD potential approximation of the Debye model and the IS model to make a comparative analysis of the results obtained from these models.

The paper is organized as follows: In Sec. II, we introduce the screening models that are considered in the calculations for the description of the atomic spectra and Sec. III describes the RCC method briefly. In Sec. IV, we present our results and compare with other available data. These results are finally summarized in Sec. V. Unless stated otherwise, we have used atomic units (a.u.) through out the paper.

II. PLASMA MODELS

We describe below the salient features of the models that have been adopted to account for the screening effects in the considered Al systems. We also give explicitly the expression for the two-body screening Debye potential in the multipole expansion form. Formulas to estimate the Debye length for the Debye potential and radius for the IS model are also given.

A. Debye model

In the weakly coupled plasma, screened potential experienced by an electron located at r_i in an atomic system due to the presence of other free electrons inside the plasma is given as [40] follows:

$$V_{\rm eff}(r_i) = e^{-r_i/D} V_{\rm nuc}(r_i) + \sum_{j \geqslant i}^{N} \frac{e^{-r_{ij}/D}}{r_{ij}}, \tag{1}$$

where $V_{\rm nuc}(r_i)$ is the nuclear potential, N is the number of bound electrons, and D is the Debye screening length. The expression to determine D for a plasma having temperature T and ion density n_i is given by

$$D = \left[\frac{k_{\rm B} T}{4\pi(1+Z)n_i} \right]^{1/2} \tag{2}$$

for the Boltzmann constant $k_{\rm B}$ and the nuclear charge Z.

The Debye potential is a long-range potential where vanishing boundary conditions are satisfied at infinity. Owing to the complicated derivation of the two-body screening potential and difficulties to perform their calculations, most of the earlier works, that were dealt with in the lighter atomic systems, had incorporated the Debye screenings only in the electron-nucleus potential. In our calculations, we refer to this as SD potential approximation. In this approach Eq. (1) is

given by

$$V_{\rm eff}(r_i) = e^{-r_i/D} V_{\rm nuc}(r_i) + \sum_{j\geqslant i}^{N} \frac{1}{r_{ij}}. \tag{3}$$

Since the considered Al ions have more than four electrons, it is anticipated that the two-body correlation effects can be significant. So it is imperative to account for the screening effects in the two-body interaction term. When the exact effective potential given by Eq. (1) is taken then we refer to the approach as NSD potential approximation. For a comprehensive understanding, we consider both cases to make a comparative study.

Again the nuclear potential $V_{\rm nuc}(r)$ is often estimated for the spectroscopy study of the plasma-embedded atomic systems by considering the nucleus as a pointlike object. In this case, it yields

$$V_{\rm nuc}(r) = -\frac{Z}{r}. \tag{4}$$

To have a more realistic potential, we use the standard Fermi charge distribution to describe the finite size of the nucleus as given by

$$\rho_{\rm nuc}(r) = \frac{\rho_0}{1 + e^{(r-b)/a}} \tag{5}$$

for the normalization factor ρ_0, the half-charge radius b, and $a = 2.3/4(\ln 3)$ is related to the skin thickness. The parameter b is evaluated using the relation

$$b = \sqrt{\frac{5}{3} r_{\rm rms}^2 - \frac{7}{3} a^2 \pi^2} \tag{6}$$

with the appropriate value of the root-mean-square radius of the nucleus $r_{\rm rms}$, which is estimated using the empirical formula

$$r_{\rm rms} = 0.836 A^{1/3} + 0.570 \tag{7}$$

in femtometers for the atomic mass A. In this case, the nuclear potential yields the form [41]

$$V_{\rm nuc}(r_i) = -\frac{Z}{\mathcal{N} r_i} \times \begin{cases} \frac{1}{b}\left[\frac{3}{2} + \frac{a^2\pi^2}{2b^2} - \frac{r^2}{2b^2} + \frac{3a^2}{b^2} P_2^+ \frac{6a^3}{b^2 r}(S_3 - P_3^+)\right] & \text{for } r_i \leqslant b \\ \frac{1}{r_i}\left[1 + \frac{a62\pi^2}{b^2} - \frac{3a^2 r}{b^3} P_2^- + \frac{6a^3}{b63}(S_3 - P_3^-)\right] & \text{for } r_i > b, \end{cases} \tag{8}$$

where the factors are

$$\mathcal{N} = 1 + \frac{a^2\pi^2}{b^2} + \frac{6a^3}{b^3} S_3$$

$$\text{with} \quad S_k = \sum_{l=1}^{\infty} \frac{(-1)^{l-1}}{l^k} e^{-lb/a}$$

$$\text{and} \quad P_k^{\pm} = \sum_{l=1}^{\infty} \frac{(-1)^{l-1}}{l^k} e^{\pm l(r-b)/a}. \tag{9}$$

The two-body screened potential is expressed as

$$V_{ee}(r_i, r_j) = \sum_{j\geqslant i}^{N} \frac{1}{r_{ij}} e^{-r_{ij}/D} = \frac{4\pi}{\sqrt{r_i r_j}} \sum_{l=0}^{\infty} I_{l+\frac{1}{2}}\left(\frac{r_<}{D}\right) K_{l+\frac{1}{2}}\left(\frac{r_>}{D}\right) \times \sum_{m=-l}^{l} Y_{lm}^*(\theta,\phi) Y_{lm}(\theta,\phi), \tag{10}$$

where $I_{l+\frac{1}{2}}$ and $K_{l+\frac{1}{2}}$ are the modified Bessel functions of the first and second kind, respectively. $r_> = \max(r_i, r_j)$; $r_< = \min(r_i, r_j)$, and $Y_{lm}(\theta,\phi)$ are the spherical harmonics of rank l. The above potential is solved in a similar way as the Coulomb potential $1/r_{ij}$ is being evaluated in common atomic structure calculations.

B. Ion-sphere model

In the strongly coupled plasma, the effective potential of the plasma-embedded atomic system is given by [42]

$$V_{\rm eff}^{\rm IS}(r_i) = \frac{(\mathrm{Z} - \mathrm{N})}{2R}\left[3 - \left(\frac{r_i}{\mathrm{R}}\right)^2\right], \tag{11}$$

where Z, N, and R represent the nuclear charge, the charge state of the ion, and the ion-sphere radius, respectively. Here R is related to the ion density $n_{\rm ion}$ as

$$\mathrm{R} = \left(\frac{3}{4\pi n_{\rm ion}}\right)^{1/3}. \tag{12}$$

Note that though it appears in the above expressions as if the plasma temperature dependence is absent, effects due to plasma temperature are taken into account in determining the free-electron distribution while deriving the expression for the above radius [2]. Unlike the case of the Debye model, a finite boundary condition $[\psi(r)|_{\rm R} = 0]$ is imposed in the IS model [42]. This boundary condition indirectly brings in the effect of the external plasma confinement due to the neighboring ions.

III. METHOD OF CALCULATIONS

To carry out the atomic wave function calculations in the considered Al species, we use the Hamiltonian in the SD model given by

$$H = \sum_{i=1}^{N} [c\vec{\alpha}_i \cdot \vec{p}_i + (\beta - 1)c^2 + e^{-r_i/D} V_{\rm nuc}(r_i)] + \frac{1}{2}\sum_{i,j} \frac{1}{r_{ij}}, \tag{13}$$

in the NSD model given by

$$H = \sum_{i=1}^{N} [c\vec{\alpha}_i \cdot \vec{p}_i + (\beta - 1)c^2 + e^{-r_i/D} V_{\rm nuc}(r_i)] + \frac{1}{2}\sum_{i,j} \frac{e^{-r_{ij}/D}}{r_{ij}}, \tag{14}$$

TABLE I. Calculated ionization potentials (IPs) and excitation energies (EEs) of Al I, Al III, Al IX, and Al XI using the CCSD method. These values are compared with the available values in the NIST database [39]. All the quantities are given in cm^{-1}.

Al I			Al III			Al IX			Al XI		
State	Present	NIST	State	Present	NIST	State	Present	NIST	State	Present	NIST
					Ionization potentials						
$3P_{1/2}$	47777.96	48278.48	$3S_{1/2}$	229311.73	229445.7	$2P_{1/2}$	2664482.59	2663340	$2S_{1/2}$	3565617.36	3565010
					Excitation energies						
$3P_{3/2}$	212.72	112.06	$3P_{1/2}$	53673.29	53682.93	$2P_{3/2}$	5853.17	4890	$2P_{1/2}$	176124.76	176019
$3D_{3/2}$	33038.43	32435.45	$3P_{3/2}$	53920.25	53916.60	$3S_{1/2}$	1500857.39	1501020	$2P_{3/2}$	182372.76	181808
$3D_{5/2}$	33027.14	32436.79	$3D_{3/2}$	115955.41	115958.50	$3P_{1/2}$	1574228.67		$3S_{1/2}$	2020890.43	2020450
$4S_{1/2}$	24943.09	25347.75	$3D_{5/2}$	115954.15	115956.21	$3P_{3/2}$	1575551.79		$3S_{1/2}$	2069289.06	2068770
$4P_{1/2}$	32522.94	32949.80	$4S_{1/2}$	126062.54	126164.05	$3D_{3/2}$	1643032.22	1642140	$3P_{3/2}$	2071130.56	2070520
$4P_{3/2}$	32543.51	32965.64	$4P_{1/2}$	143537.40	143633.38	$3D_{5/2}$	1643379.69	1642380	$3D_{3/2}$	2088662.63	2088100
			$4P_{3/2}$	143622.20	143713.50	$4S_{1/2}$	2043518.52		$3D_{5/2}$	2089195.23	2088530
						$4P_{1/2}$	2071861.95		$4S_{1/2}$	2706972.19	2705700
						$4P_{3/2}$	2072401.64		$4P_{1/2}$	2726831.30	2726120
									$4P_{3/2}$	2727605.74	2726910

and in the IS model given by

$$H = \sum_{i=1}^{N} \left[c\vec{\alpha}_i \cdot \vec{p}_i + (\beta - 1)c^2 + V_{\text{eff}}^{\text{IS}}(r_i) \right] + \frac{1}{2} \sum_{i,j} \frac{1}{r_{ij}}, \tag{15}$$

where $\vec{\alpha}$ and β are the Dirac matrices and c is the velocity of light.

The wave functions of the states of the considered atomic systems are evaluated by classifying the orbitals into a closed core and a valence orbital. In this approach the wave functions are expressed in the RCC ansatz as [43,44]

$$|\Psi_v\rangle = e^T\{1 + S_v\}|\Phi_v\rangle = e^T\{1 + S_v\}a_v^\dagger|\Phi_c\rangle, \tag{16}$$

where T and S_v are the RCC excitation operators that excite electrons from the core and core along with the valence orbitals to the virtual space, respectively. Here $|\Phi_c\rangle$ and $|\Phi_v\rangle$ are the Dirac-Hartree-Fock (DHF) wave functions of the closed core and the closed core with the valence orbital, respectively. In this work, we have considered only the single and double excitations, denoted by the subscripts 1 and 2, respectively, in the RCC calculations (known as the CCSD method) by expressing

$$T = T_1 + T_2 \quad \text{and} \quad S_v = S_{1v} + S_{2v}. \tag{17}$$

The amplitudes of these operators are evaluated using the equations

$$\langle \Phi_c^* | \overline{H}_N | \Phi_c \rangle = 0 \tag{18}$$

and

$$\langle \Phi_v^* | \left(\overline{H}_N - \Delta E_v \right) S_v | \Phi_v \rangle = -\langle \Phi_v^* | \overline{H}_N | \Phi_v \rangle, \tag{19}$$

where $|\Phi_c^*\rangle$ and $|\Phi_v^*\rangle$ are the excited-state configurations, here up to doubles, with respect to the $|\Phi_c\rangle$ and $|\Phi_v\rangle$ DHF wave functions, respectively, and $\overline{H}_N = (H_N e^T)_l$, where the subscript l represents the linked terms only. In the above expression, ΔE_v is the attachment energy of the electron in the valence orbital v. In the *ab initio* approach, the ΔE_v value is determined using the expression

$$\Delta E_v = \langle \Phi_v | \overline{H}_N \{1 + S_v\} | \Phi_v \rangle. \tag{20}$$

As can be seen, both Eqs. (19) and (20) need to be solved simultaneously. Hence, Eq. (19) is also nonlinear in the S_v operator, although it does not appear to be so.

IV. RESULTS AND DISCUSSION

In this section, we present results obtained for IPs and EEs of Al ions obtained using the RCC method separately for Debye and ion-sphere potentials. A detailed comparative analysis has been made for the results from both the SD and NSD potential approximations. In order to verify accuracies in our results obtained employing the RCC method, we compare the IPs and EEs of the isolated Al atom and its ions with the listed values of the National Institute of Science and Technology (NIST) database [39] in Table I. This is done except for the EEs of the $3P_{3/2}$ and $4P_{3/2}$ states of Al IX, where the NIST data are not available. We also determine the fine structure splittings (FSs) from these values and present them in the same table. We observe good agreement between the calculated and the experimental results, except among the FS transitions. This may be due to the fact that higher-order relativistic correlations are expected to contribute to these transitions substantially. Agreement among the EEs of the other transitions is an indication that the determined IPs, EEs, and FSs of the plasma-embedded Al systems can also be of similar accuracies by taking confidence in the validity of the considered models.

A. Results from the Debye model

We perform the calculations of IPs by varying the D value, which corresponds to different plasma density (n_i) and plasma temperature (T), in the Debye model. As described, the plasma screening effects are included using both the SD potential and NSD potential approximations. A comparison among the results from these two approximations can demonstrate the role

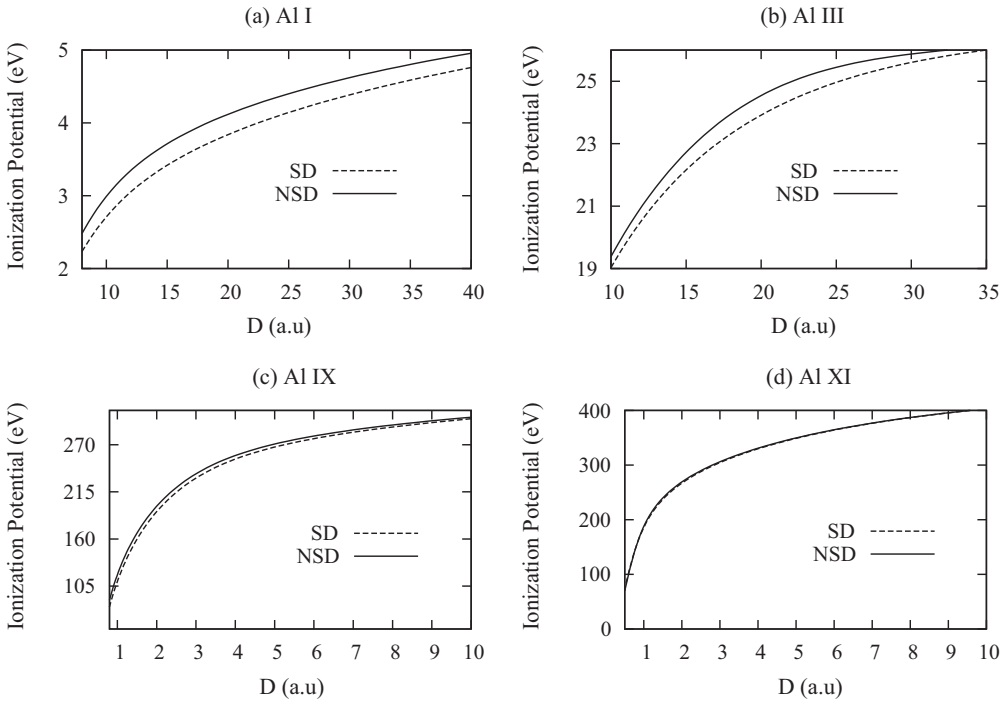

FIG. 1. Variation in the ionization potentials (IPs) with the Debye screening length in (a) Al I, (b) Al III, (c) Al IX, and (d) Al XI.

of plasma screening through the electron-electron correlation effects in the considered systems. To examine this, we vary the D value from 5.0 a.u. to 100 a.u. in Al I, from 3 a.u. to 100 a.u. in Al III, from 0.6 a.u. to 13.6 a.u. in Al IX, and from 0.5 a.u. to 13.6 a.u. in Al XI. In Fig. 1, we show changes in IPs with the D values in Al I, Al III, Al IX, and Al XI for both the SD and NSD potential approximations. As expected, the IPs decrease smoothly with decrease in the D value in all the systems; this is one of the unique properties of the plasma-embedded atomic systems [13–16]. One can clearly observe from these plots that the differences in IPs between the SD and NSD potential approximations are large in Al I and gradually it gets reduced when Al is more ionized. In Al I, the results from both approximations differ substantially, implying it is imperative to include electron correlation effects accurately in the many-electron systems. It can also be noticed from the results that the differences in Al I and Al III are slightly larger for the intermediate range of D. This may be because of the fact that with the increase of screening effect, the electrons become more relaxed at the intermediate values of D. When the D value is increased further, the electrons start seeing stronger plasma screening effects through the nuclear potential. Hence, for the large D values the differences between the IPs gradually decrease in both the SD and NSD potential approximations. To get a quantitative realization of variation of IPs with the D values, we quote IPs of all the considered ions for some selective values of D in Table II using both the SD and NSD potential approximations. Differences between the results from both the approximations have been given as ΔIP in the same table.

From Fig. 1, we obtain the IPDs to be 2.52 eV, 19.85 eV, 233.41 eV, and 368.95 eV at D values of 10 a.u., 3 a.u., 0.8 a.u., and 0.5 a.u. for Al I, Al III, Al IX, and Al XI, respectively, in the NSD potential approximation.

To understand the variation in the excitation energies of plasma-embedded ions, we also investigate variation in the first

TABLE II. A list of IPs (in cm^{-1}) for some arbitrary values of Debye length (D in a.u.) obtained using the SD and NSD potential approximations in the Debye model. Differences in the results from both approximations are given as ΔIP in cm^{-1}.

Ion	D	SD	NSD	ΔIP
Al I	75	44117.72	44875.06	757.34
	65	43571.82	44433.20	861.38
	30	38975.59	40622.00	1646.41
	20	34993.49	37176.15	2182.66
	10	24592.35	27444.05	2851.70
Al III	60	218698.15	218518.13	180.02
	40	213538.94	213254.15	284.79
	30	208475.70	208076.78	398.92
	10	168520.85	166833.28	1687.57
	5	122568.03	118492.86	4075.17
	3	76603.26	68983.50	7619.76
Al IX	10	2458618.42	2471216.96	12598.54
	5	2262628.87	2286219.55	23590.68
	2	1726164.27	1773863.71	47699.44
	1.5	1462681.28	1519187.01	56505.73
	1.0	1003850.78	1071138.01	67287.23
	0.8	710695.14	779068.71	68373.57
Al XI	12	3368721.32	3368613.91	107.41
	5	3106688.38	3106348.89	339.49
	3	2825588.51	2824867.62	720.89
	1.5	2201132.03	2198937.43	2194.6
	0.6	884330.29	874154.68	10175.61
	0.5	598991.96	585398.94	13593.02

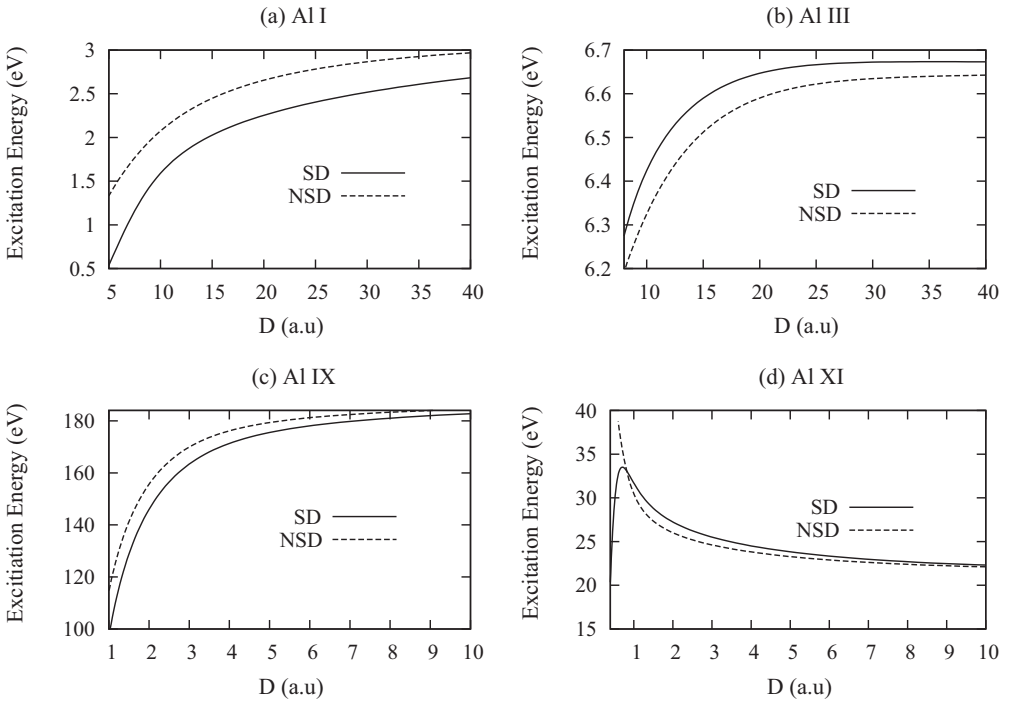

FIG. 2. Variation in the first EE (in cm^{-1}) of (i) Al I, (ii) Al III, (iii) Al IX, and (iv) Al XI with the Debye screening length D (in a.u.).

excited-state energies of the Al I, Al III, Al IX, and Al XI ions with the Debye length. In Fig. 2, we have plotted them against the D values considering both the SD and NSD potential approximations. One can infer from this figure that the EEs of the excited states in the plasma-embedded Al systems decrease with decreasing values of D, except in the Al XI ion. We find the situation is quite different in the Al XI ion, where the EE of the $2P_{1/2}$ state increases with the increasing screening strength. However, at the very high screening region, this EE starts decreasing at some critical D value in the SD approximation. This behavior was also seen in the hydrogenlike ions [6] and lithiumlike ions [45] in the Debye model studies, whereas in the NSD potential approximation, this behavior disappears. Therefore, it implies that the use of NSD potential in the Debye model reduces the electron-electron screening effects that are overestimated in the SD model approximation in the systems having many electrons. Thus, it demonstrates the importance of accounting for the plasma screening effects through the two-body interaction term in the many-electron systems accurately. Another aspect that can be observed from the analysis of EEs in the considered systems is that the differences between the EEs obtained using the SD and NSD potential approximations are larger than their IPs, as seen in Figs. 1 and 2. This means that the screening effects affect the ground and the excited states differently.

B. Results from the IS model

Here, we proceed with presenting the results from the IS model by carrying out the calculations using the RCC method. These results are supposed to explain the systems in the strong-coupling plasma environment. In Fig. 3, we have plotted the IPs of the Al III, Al IX, and Al XI ions with different IS radii. In this model, the IS radius is varied from 4 a.u. to 11.3 a.u., 3 a.u. to 10 a.u., and 4.48 a.u. to 19.32 a.u. in the Al III, Al IX, and Al XI ions, respectively. From the plot we can see that the IPs decrease monotonically with decreasing the ion-sphere radius R. The decaying trends in the plots mean growing instability in the system with the rise of ion density in the strong plasma environment. A similar pattern was also observed by Sil *et al.* [46] for the plasma-embedded Al^{11+} ion in the same IS model analysis.

In the same spirit as of Debye model, we have also investigated the trends in the EEs of the first excited states of all the considered atomic systems in the IS model by varying R. The variation of the EE of the $3P_{1/2}$ state in the Al III ion with IS

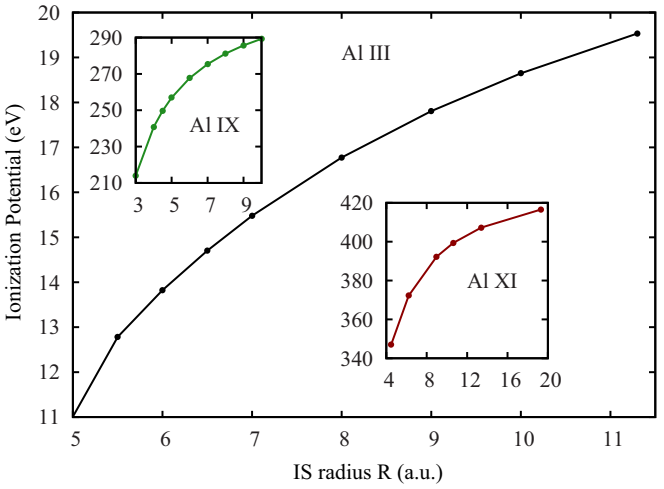

FIG. 3. Variation of ionization potential (IP) in the Al III ion with the ion-sphere radius R (in a.u.). Inset plots are shown for the Al IX and Al XI ions.

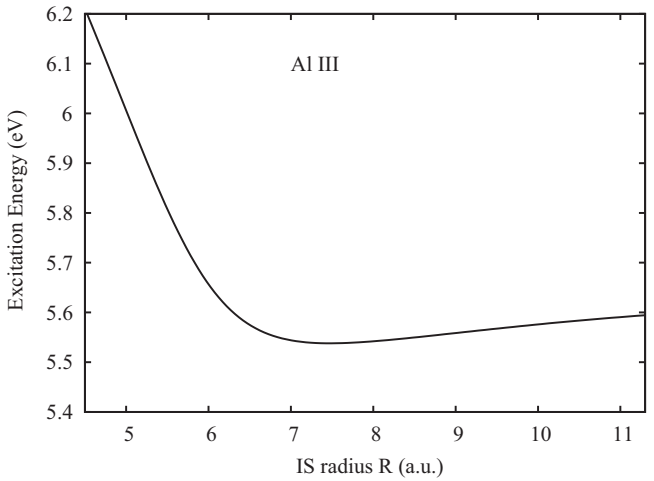

FIG. 4. Variation of EE of the $3P_{1/2}$ state in the Al III ion with the IS radius R (a.u.).

radius shows a very peculiar result, as shown in Fig. 4. Initially, the EEs of the $3P$ states decrease with decreasing value of IS radius, and then they suddenly rise at certain critical values of R. Similar trends are also seen in the higher excited states of the Al III ion.

In Figs. 5 and 6, we have plotted the variation of EEs in the Al IX and Al XI ions, respectively. From Fig. 5, we find that in the Al IX ion EE of the $3S_{1/2}$ state decreases with decreasing value of IS radius, whereas in the Al XI ion, EE of the $2P_{1/2}$ state increases with decreasing radius of IS. From these findings in the high-density plasma, we conclude that for low ionized systems, like Al III, the transition spectra are initially redshifted and towards very high density regions, it becomes blueshifted. In contrast, the highly ionized ions, such as Al IX and Al XI, show blueshift in the spectral lines in the transitions between the states having the same principal quantum numbers and redshifted in the transitions involving states with different principal quantum numbers.

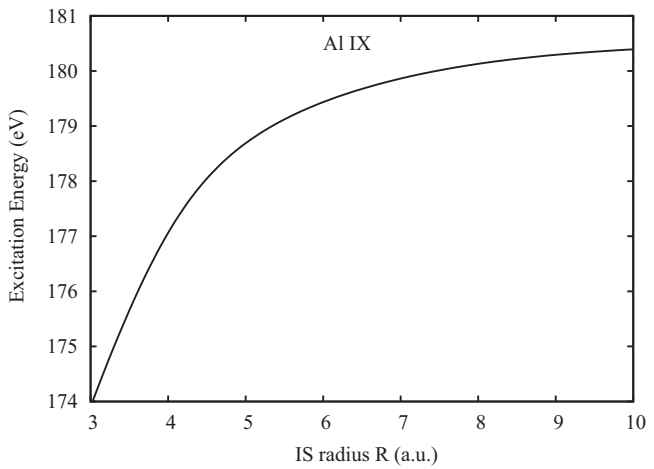

FIG. 5. Variation of EE of the $3S_{1/2}$ state in the Al IX ion with the IS radius R (a.u.).

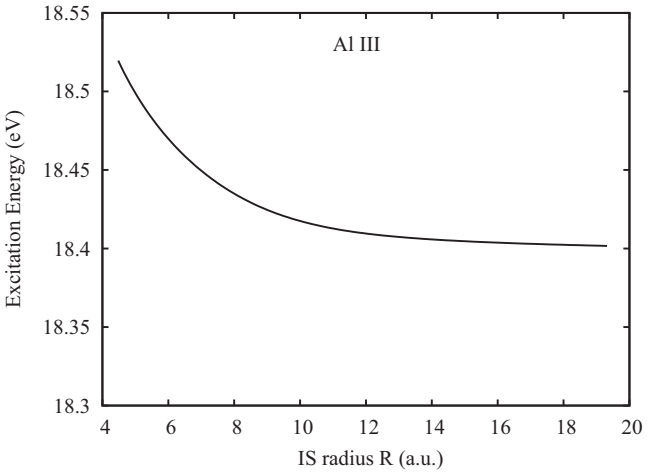

FIG. 6. Variation of EE of the $2P_{1/2}$ state in the Al XI ion with IS radius R (a.u.).

C. Debye versus IS model results

Though it is well known that the Debye model describes well the weakly coupled plasma and the IS model describes appropriately the strongly coupled plasma, we just wanted to investigate the validity of both models in similar plasma conditions. For this purpose, we have calculated the IPDs of the Al III and Al XI ions under the same experimental plasma conditions using both the Debye model and the IS model at the intermediate plasma coupling. Under the experimental condition [47] with the ion density $n_i = 0.2 \times 10^{21}$/cc and the temperature at 20 eV (which corresponds to $D = 11.36$ a.u.

TABLE III. Comparison of EEs (case I) obtained using the IS model with radius $R = 20$ a.u. and Debye model with NSD potential approximation for $D = 11.3$ a.u. that corresponds to the experimental conditions with $T = 20$ eV and $n_i = 0.2 \times 10^{21}$/cc. In another case (case II), the above quantities are compared using the IS model with radius $R = 16$ a.u. and Debye model with NSD potential approximation for $D = 13.6$ a.u. corresponding to the experimental conditions with $T = (58 \pm 4)$ eV and $n_i = 0.4 \times 10^{21}$/cc.

		Experimental	EE (in cm^{-1})	
Ion	State	condition	IS model	Debye model
Al III	$3P_{1/2}$		45349.90	52819.41
	$3P_{3/2}$		45534.82	53056.49
	$3D_{3/2}$	Case I	100971.21	113316.78
	$3D_{5/2}$		100970.98	113315.68
	$4S_{1/2}$		115413.04	120263.59
	$4P_{1/2}$		130384.45	136394.76
	$4P_{3/2}$		130447.22	136468.07
Al XI	$3S_{1/2}$		1995874.47	2016739.20
	$3P_{1/2}$		2036363.33	2065474.87
	$3P_{3/2}$	Case II	2038140.30	2067306.84
	$3D_{3/2}$			2085870.23
	$3D_{5/2}$			2086399.55
	$4S_{1/2}$		2679621.16	2697199.34
	$4P_{1/2}$		2692124.54	2717306.72
	$4P_{3/2}$		2692875.54	2718069.23

and $R = 20$ a.u.), the obtained IPDs of the Al III ion are 6.6 eV and 5.8 eV in the Debye and IS models, respectively. Similarly, with the experimental plasma condition [48] with $n_i = 0.4 \times 10^{21}$/cc and $T = 58 \pm 4$ eV (corresponding to $D = 13.6$ a.u. and $R = 16$ a.u.), the IPD of Al XI are found to be 21.60 eV and 24.3 eV in the Debye and IS models, respectively. We have also estimated EEs of many low-lying excited states of the Al III and Al XI ions using these two models under the above experimental conditions and have given them in Table III for comparison purposes. We find a quite good agreement in the results from both the models in Al III and Al XI, while results from the Debye model are relatively larger. The above plasma coupling strengths under the experimental conditions ($n_i = 0.2 \times 10^{21}$/cc, $T =$ 20 eV) and ($n_i = 0.4 \times 10^{21}$/cc, $T = 58 \pm 4$ eV) are about 2.8 and 1.2, respectively; they are in the intermediate range of classifying as either weakly coupled plasma (i.e., $\Gamma \ll 1$) or strongly coupled plasma (i.e., $\Gamma \geqslant 10$). So, in this intermediate region one would expect both models to give comparatively similar results. We anticipate that results obtained using the IS model are more valid here, as the plasma couplings corresponding to the above plasma conditions are larger than 1, where the Debye model may not be able to describe the systems appropriately.

V. CONCLUDING REMARKS

In this work, we have investigated the electronic structures of Al atoms and some of their ions both in weak- and strong-coupling plasma environments considering the Debye and ion-sphere models, respectively. Furthermore, we have investigated differences in the results considering the plasma screening effects in the electron-electron repulsion with the spherical potential and nonspherical potential approximations within the Debye model to estimate ionization potential depressions and excitation energies of the considered systems. We find significant differences in the results in the systems having more electrons. It also predicts more stability in the atomic systems when the exact screening effects are taken into account. A similar analysis has also been carried out to analyze structures of the Al ions in the strongly coupled plasma using the ion-sphere model. In this model, we find the highly ionized ions show blueshifts in the transitions among the states with the same principal quantum numbers and redshifts with the decreasing values of ion-sphere radius. Out of keenness, we have also applied both the Debye and ion-sphere models to carry out calculations of the ionization potential depressions and excitation energies in the Al III and Al XI ions considering the plasma conditions that fall in the intermediate coupling plasma strengths. We find from this investigation that the ionization potential depressions for the Al III and Al XI ions obtained using both plasma models reasonably agree with each other, but the Debye model predicts higher values.

ACKNOWLEDGMENTS

M.D. thanks Council of Scientific and Industrial Research, India for financial support. Some of the computations were carried out using the Vikram-100 HPC cluster at the Physical Research Laboratory, Ahmedabad.

[1] M. S. Murillo and J. C. Weisheit, Phys. Rep. **302**, 1 (1998).
[2] D. Salzman, *Atomic Physics in Hot Plasma* (Oxford University Press, New York, 1998).
[3] J. D. Lindl, P. Amendt, and R. L. Berger, Phys. Plasmas **11**, 339 (2004).
[4] S. Ichimaru, Rev. Mod. Phys. **54**, 1017 (1982).
[5] D. Bielinska-Waz, J. Karwowski, B. Saha, and P. K. Mukherjee, Phys. Rev. E **69**, 016404 (2004).
[6] Y. Y. Qi, J. G. Wang, and R. K. Janev, Phys. Rev. A **78**, 062511 (2008).
[7] B. Saha, P. K. Mukherjee, D. Bielinska-Waz, and J. Karwowski, J. Quant. Spectrosc. Radiat. Transf. **92**, 1 (2005).
[8] Y. Y. Qi, Y. Wu, J. G. Wang, and Y. Z. Qu, Phys. Plasmas **16**, 023502 (2009).
[9] B. Saha, P. K. Mukherjee, and G. H. F. Diercksen, Astron. Astrophys. **396**, 337 (2002).
[10] S. Paul and Y. K. Ho, Phys. Plasmas **16**, 063302 (2009).
[11] J. K. Saha, S. Bhattacharyya, T. K. Mukherjee, and P. K. Mukherjee, J. Phys. B **42**, 245701 (2009).
[12] M. Das, M. Das, R K. Chaudhuri, and S. Chattopadhyay, Phys. Rev. A **85**, 042506 (2012).
[13] D. R. Inglis and E. Teller, Astrophys. J. **90**, 439 (1939).
[14] R. P. Feynman, N. Metropolis, and E. Teller, Phys. Rev. **75**, 1561 (1949).
[15] G. Ecker and W. Kröll, Phys. Fluids **6**, 62 (1963).
[16] J. C. Stewart and K. D. Pyatt, Jr., Astrophys. J. **144**, 1203 (1966).
[17] K. Wang, Z. Shi, Y. Shi, J. Bai, J. Wu, and S. Jia, Phys. Plasmas **22**, 062709 (2015).
[18] J. E. Bailey *et al.*, Phys. Plasmas **16**, 058101 (2009).
[19] M. J. Seaton, Y. Yan, D. Mihalas, and A. K. Pradhan, Mon. Not. R. Astron. Soc. **266**, 805 (1994).
[20] J. Eschner *et al.*, J. Opt. Soc. Am. B **20**, 1003 (2003).
[21] E. Storm, Fusion J. Energy **7**, 131 (1988).
[22] J. C. Riordan and J. S. Pearlman, Appl. Phys. Lett. **39**, 543 (1981).
[23] E. Pérez-Tijerina, J. Bohigas, and R. Machorro, Rev. Mex. Fís. **51**, 153 (2005).
[24] S. S. Ciobanu, C. Negutu, M. Stafe, I. Vladoiu, V. Pais, V. Stancalie, and N. N. Puscas, in *35th EPS Conference on Plasma Phys., Hersonissos, 9–13 June 2008*, ECA, Vol. 32D, P-5.144 (1-4), (2008).
[25] D. J. Hoarty, P. Allan, S. F. James, C. R. D. Brown, L. M. R. Hobbs, M. P. Hill, J. W. O. Harris, J. Morton, M. G. Brookes, R. Shepherd, J. Dunn, H. Chen, E. Von Marley, P. Beiersdorfer, H. K. Chung, R. W. Lee, G. Brown, and J. Emig, Phys. Rev. Lett. **110**, 265003 (2013).
[26] O. Ciricosta, S. M. Vinko, H. K. Chung, B. I. Cho, C. R. D. Brown, T. Burian, J. Chalupsky, K. Engelhorn, R. W. Falcone, C. Graves, V. Hajkova, A. Higginbotham, L. Juha, J. Krzywinski, H. J. Lee, M. Messerschmidt, C. D. Murphy, Y. Ping, D. S. Rackstraw, A. Scherz *et al.*, Phys. Rev. Lett. **109**, 065002 (2012).
[27] J. Zeng, F. Jin, J. Yuan, Q. Lu, and Y. Sun, Phys. Rev. E **62**, 7251 (2000).
[28] P. Feng, J. Gang, and Z. Zheng-He, Chin. Phys. Lett. **23**, 3245 (2006).

[29] T. R. Preston, S. M. Vinko, O. Ciricosta, H.-K. Chung, R. W. Lee, and J. S. Wark, High Energy Density Phys. **9**, 258 (2013).
[30] S. Kiyokawa, J. At. Mol. Phys. **2014**, 431592 (2014).
[31] M. Nantel, G. Ma, S. Gu, C. Y. Cote, J. Itatani, and D. Umstadter, Phys. Rev. Lett. **80**, 4442 (1998).
[32] K. Nazir, S. J. Rose, A. Djaoui, G. J. Tallents, M. G. Holden, P. A. Norreys, P. Fews, J. Zhang, and F. Failles, Appl. Phys. Lett. **69**, 3686 (1996).
[33] B. A. Hammel, C. J. Keane, M. D. Cable, D. R. Kania, J. D. Kilkenny, R. W. Lee, and R. Pasha, Phys. Rev. Lett. **70**, 1263 (1993).
[34] A. Szabo and N. Ostuland, *Modern Quantum Chemistry*, 1st ed., rev. (Dover Publications, Inc., Mineola, NY, 1996).
[35] I. Shavitt and R. J. Bartlett, *Many-Body Methods in Chemistry and Physics* (Cambridge University Press, Cambridge, UK, 2009).
[36] O. Čertík and P. Winkler, Int. J. Quant. Chem. **113**, 2012 (2013).
[37] J. S. Yoon and Y. D. Jung, Phys. Plasmas **3**, 3291 (1996).
[38] F. A. Gutierrez and J. Diaz-Valdes, J. Phys. B: Atom. Mol. Phys. **27**, 593 (1994).
[39] See http://physics.nist.gov/PhysRefData/ASD.
[40] A. I. Akhiezer, I. A. Akhiezer, R. A. Polovin, A. G. Sitenko, and K. N. Stepanov, *Plasma Electrodynamics, Linear Response Theory* (Pergamon, Oxford, 1975), Vol. 1.
[41] G. Estevez and L. B. Bhuiyan, Am. J. Phys. **53**, 450 (1985).
[42] B. F. Rozsnyai, Phys. Rev. A **43**, 3035 (1991).
[43] D. K. Nandy and B. K. Sahoo, Phys. Rev. A **88**, 052512 (2013).
[44] B. K. Sahoo, Phys. Rev. A **93**, 022503 (2016).
[45] M. Das, B. K. Sahoo, and S. Pal, J. Phys. B: At. Mol. Opt. Phys. **47**, 175701 (2014).
[46] A. N. Sil, J. Anton, S. Fritzsche, P. K. Mukherjee, and B. Fricke, Eur. Phys. J. D **55**, 645 (2009).
[47] G. Winhart, K. Eidmann, C. A. Iglesias, and A. Bar-Shalom, Phys. Rev. E **53**, R1332 (1996).
[48] T. S. Perry, S. J. Davidson, F. J. D. Serduke, D. R. Bach, C. C. Smith, J. M. Foster, R. J. Doyas, R. A. Ward, C. A. Iglesias, F. J. Rogers, J. Abdallah, R. E. Stewart, J. D. Kilkenny, and R. W. Lee, Phys. Rev. Lett. **67**, 3784 (1991).